






ARTICLE

<https://doi.org/10.1038/s42004-019-0122-7>

OPEN

# Micro-Raman imaging of isomeric segregation in small-molecule organic semiconductors

Chiung-Wei Huang <sup>1</sup>, Xiao You <sup>2</sup>, Peter J. Diemer<sup>3</sup>, Anthony J. Petty II<sup>4</sup>, John E. Anthony <sup>4</sup>, Oana D. Jurchescu <sup>3</sup> & Joanna M. Atkin <sup>1</sup>

Charge transport in organic semiconductors is highly sensitive to film heterogeneity and intermolecular interactions, but probing these properties on the length scales of disorder is often difficult. Here we use micro-Raman spectroscopy to assign vibrational modes of isomerically pure *syn* and *anti* 2,8-difluoro-5,11-bis(triethylsilylethynyl)anthradithiophene (diF-TES ADT) by comparing to density functional theory calculations. With polarization-dependent measurements, we determine the orientation of crystallites in pure isomers. In mixed-isomer samples, we observe narrow linewidths and superposition spectra, indicating coexistence of isomerically pure sub-domains on length scales smaller than the probe area. Using the ring breathing modes close to  $1300\text{ cm}^{-1}$  as indicators of the pure isomer crystalline sub-domains, we image their spatial distribution with 200-nm resolution. These results demonstrate the power of micro-Raman spectroscopy for investigating spatial heterogeneities and clarifying the origin of the reduced charge carrier mobility displayed in mixed-isomer diF-TES ADT.

<sup>1</sup>Department of Chemistry, University of North Carolina, Chapel Hill, NC 27599, USA. <sup>2</sup>Department of Applied Physical Sciences, University of North Carolina, Chapel Hill, NC 27599, USA. <sup>3</sup>Department of Physics, Wake Forest University, Winston-Salem, NC 27109, USA. <sup>4</sup>Department of Chemistry, University of Kentucky, Lexington, KY 40506, USA. Correspondence and requests for materials should be addressed to J.M.A. (email: [jatkin@ad.unc.edu](mailto:jatkin@ad.unc.edu))

Organic  $\pi$ -conjugated systems are appealing for ultrathin, flexible, and low-cost electronic devices applications. Organic thin-film transistors (OTFTs), for example, can be incorporated in flat-panel displays, radio-frequency identification tags, conformable sensor arrays, memory devices, and health monitoring systems when their performance reaches the levels required by such applications<sup>1–4</sup>. The charge carrier mobility, and thereby device performance in OTFTs, is very sensitive to the molecular structure of the organic semiconductor, as well as its solid state packing and microstructure, which are highly dependent on processing conditions<sup>5–12</sup>. Control of microstructure and determination of its spatial variation is difficult, especially in the presence of multiple isomers or structures, complicating optimization of performance.

Anthrathiophene (ADT) is a small-molecule organic semiconductor that showed good electronic performance but limited solubility, which precludes its compatibility with flexible and bendable substrates<sup>13,14</sup>. Solution processability was achieved by adding side groups to the molecular backbone, as for example in 5,11-triethylsilylethynyl anthradithiophene (TES-ADTs). Unfortunately, in the absence of complicated post-processing treatments, TES ADT typically forms amorphous films with insufficient order to support high-performance OTFTs, or polymorphs that vary greatly in electrical properties<sup>15,16</sup>. Fluorinated analogs, in contrast, benefit from F–H and F–S interactions between adjacent molecules and demonstrate improved crystallinity<sup>17</sup>. The fluorinated ADT 2,8-difluoro-5,11-bis(triethylsilylethynyl)anthradithiophene (diF-TES ADT) is among the most promising molecules for incorporation in OTFTs (Fig. 1a) with a charge carrier mobility as high as  $6 \text{ cm}^2 \text{ V}^{-1} \text{ s}^{-1}$  reported in vapor grown single crystals of this material<sup>18</sup>. In solution-deposited OTFTs, the mobility varies from  $10^{-2}$  to  $5.4 \text{ cm}^2 \text{ V}^{-1} \text{ s}^{-1}$  depending on the deposition method, chemical modifications

of the surface prior to film deposition, and the dielectric<sup>19–23</sup>. diF-TES ADT films deposited on Au substrates modified with fluorinated self-assembled monolayers (SAMs) such as pentafluorobenzenethiol (PFBT), 4-(trifluoromethyl)-benzenethiol (TFBT), or 2,3,5,6-tetrafluoro-4-(trifluoromethyl)-benzenethiol (TTFP) exhibit a high degree of crystallinity, with the conjugated backbone of the molecules perpendicular to the surface substrate, as illustrated in Fig. 1b<sup>20,22</sup>. The vertical orientation was induced by selective F–H and F–S interactions between the molecule and the fluorine in the SAM surface<sup>24</sup>, an orientation that is favorable for in-plane  $\pi$ -orbital overlap and that can improve charge mobility by a factor of ten<sup>19</sup>.

With a few exceptions<sup>25–27</sup>, most studies on diF-TES ADT have looked at isomeric mixtures, due to the fact that under standard synthesis procedures, diF-TES ADT is prepared as an inseparable mixture of *syn* and *anti* isomers<sup>17</sup>. The process of separating the isomers is intensive and expensive<sup>26</sup>. Performance in as-deposited mixed-isomer molecules is lower than devices fabricated from isomerically pure molecules<sup>26,27</sup>, with the decreased mobility attributed to molecular disorder from the mixed isomers<sup>19</sup>.

Here we use micro-Raman spectroscopy to investigate the degree of crystalline order and isomeric segregation in diF-TES ADT films. We report on thin films prepared by solvent-assisted crystallization (SAC) on PFBT-treated Au electrodes, yielding improved film quality with highly ordered microstructure in the diF-TES ADT films<sup>20,28,29</sup>. Raman spectroscopy is sensitive to conjugated molecular systems, with a large scattering cross-section coupled to the  $\pi$ - $\pi^*$  modes. We utilize this high sensitivity to distinguish the *syn* and *anti* isomers, in combination with density functional theory (DFT) calculations. The sub-micron focus possible in Raman spectroscopy minimizes averaging in the molecular signatures, allowing us to resolve the coexistence of pure isomer domains within mixed-isomer thin films with spatial resolution down to 200 nm. Our results suggest that the reduced mobility in mixed-isomer devices can be attributed to the grain boundaries arising from isomeric phase segregation, rather than changes in order, orientation, or intermolecular interactions.

## Results

**Vibrational modes of pure isomers.** The experimental Raman spectra of *syn* and *anti* diF-TES ADT films on PFBT-treated Au electrodes are shown in Fig. 2, with the associated DFT calculations (gray). The calculated spectra were convolved with a Lorentzian with full-width at half-maximum bandwidth of  $2 \text{ cm}^{-1}$ . The PFBT-modified Au substrate shows a vibrational mode at  $1555 \text{ cm}^{-1}$  (Supplementary Figure 1), but the diF-TES ADT thin films were sufficiently thick that this mode was not typically observed. By comparing the experimentally obtained spectra with calculations and previous reports in five-ring small-molecule analogous, pentacene and 6,13-Bis(triisopropylsilylethynyl)pentacene (TIPS-pentacene), Raman modes of diF-TES ADT are assigned and shown in Table 1. The calculated displacement vectors for selected vibrational modes are included in Supplementary Figure 2.

In both the *syn* the *anti* isomers, the C–C stretch modes along the long axis of the molecular core appear at  $1597 \text{ cm}^{-1}$ , consistent with a previously assigned mode in pentacene ( $1596 \text{ cm}^{-1}$ )<sup>30,31</sup>. Figure 1c shows the atomic displacements, with blue arrows indicating stretching along the long axis of the conjugated backbone. A lower frequency long-axis stretching band appears as a doublet at  $1543/1529 \text{ cm}^{-1}$  for both isomers. A similar doublet appears in pentacene, where the splitting arises due to stretch motions predominantly at the central or end rings of the conjugated backbone<sup>32</sup>. In spite of the similarity in the spectral

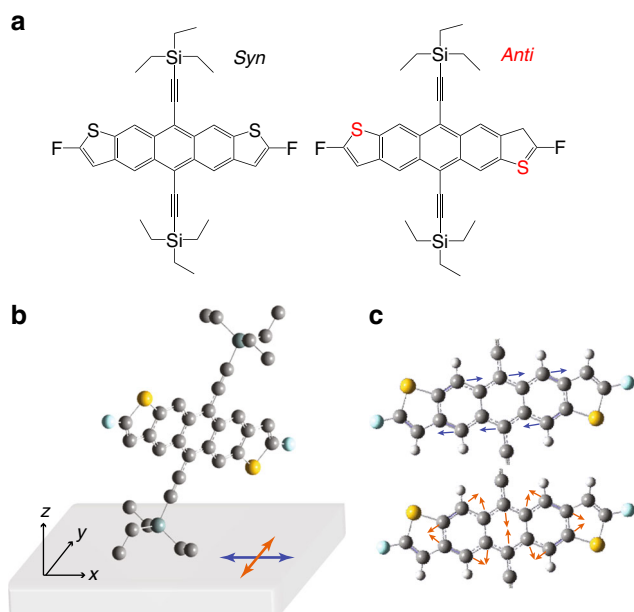


**Fig. 1** Chemical and packing structure of 2,8-difluoro-5,11-bis(triethylsilylethynyl)anthradithiophene (diF-TES ADT). **a** Chemical structure of diF-TES ADT, with *syn* (black) and *anti* (red) isomers. **b** Schematic representation of orientation of molecular on surface. The blue and orange arrows indicate the polarization directions that predominantly excite long- and short-axis vibrational modes along the conjugated backbone. **c** The displacement vectors associated with the dominant long- and short-axis stretch modes

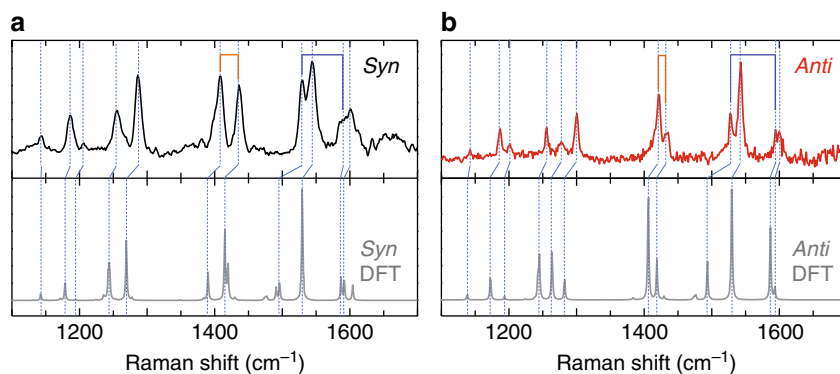


**Fig. 2** Raman spectra for pure isomers. **a** *Syn* 2,8-difluoro-5,11-bis(triethylsilylethynyl)anthradithiophene (diF-TES ADT) and **b** *anti* diF-TES ADT in the 1100–1700  $\text{cm}^{-1}$  range. Density functional theory (DFT) calculations are shown in gray. The blue lines indicate vibrational modes associated with the long axis of the acene backbone, which are relatively insensitive to the isomers. The orange lines indicate the short-axis C-C bonds, which are spectrally shifted between the *syn* and *anti* isomers

**Table 1** Raman mode assignments for the dominant peaks of *anti* and *syn* diF-TES ADT (in  $\text{cm}^{-1}$ )

<i>Anti</i>		<i>Syn</i>		Assignment	Reference	
DFT	Experiment	DFT	Experiment		Pentacene <sup>31</sup>	TIPS-pentacene <sup>38, 39</sup>
1594	1597	1604	1597	C-C ring stretch (long axis)	1596	1576
1587		1592				
		1587				
1529	1543	1529	1543	C-C ring stretch (center rings)	1498 <sup>32</sup> (center rings)	
1494	1529	1496	1529	C-C ring stretch (partial-long axis)	1532 <sup>32</sup> (end rings)	
1406	1434	1420	1436	C-C ring stretch (short axis, end rings)	1408 <sup>32</sup>	1374
		1415				
1419	1421	1390	1407	(short axis, center rings)	1370 <sup>32</sup>	
1283	1300	1269	1286	Ring breathing		
1263	1278			Ring breathing		
1245	1256	1244	1256	Ring breathing		
1193	1200	1179	1207	C-H bending (sides)	1178	1194
1172	1187	1171	1186	C-H bending		
1138	1143	1142	1143	C-H bending (ends)	1158	1158

diF-TES ADT 2,8-difluoro-5,11-bis(triethylsilylethynyl)anthradithiophene, DFT density functional theory, TIPS-pentacene 6,13-Bis(triisopropylsilylethynyl)-pentacene

positions, the calculations indicate that these frequencies correspond to different atomic motion, with the heteroatom modification suppressing terminal ring stretching and altering the distribution of atomic motion along the long axis (Supplementary Figure 2).

Vibrations of the C-C ring stretch along the short axis are significantly shifted in *syn* and *anti* isomers relative to pentacene. In the *anti* isomer, these vibrational modes occur at 1434 and 1421  $\text{cm}^{-1}$ , compared to 1436 and 1407  $\text{cm}^{-1}$  in the *syn* isomer. The band splitting is in line with previous studies on pentacene, where it is attributed to different displacements of the H atoms located at the terminal rings (1408  $\text{cm}^{-1}$ ) from the central rings (1370  $\text{cm}^{-1}$ )<sup>32</sup>. Figure 1c illustrates the atomic displacements of central rings stretching along the short axis of the conjugated backbone with orange arrows.

While pentacene exhibits no signature bands in the range 1200–1300  $\text{cm}^{-1}$ , diF-TES ADT molecules possess multiple vibrational modes, assigned as aromatic ring breathing modes. These vibrations result in uniform C-C bond length elongation. The ring-breathing mode in the *anti* isomer is found at 1300  $\text{cm}^{-1}$ , and is red-shifted to 1286  $\text{cm}^{-1}$  in the *syn* isomer. The C-H bending modes from the sides of the molecular core are also significantly blue-shifted from pentacene (1178  $\text{cm}^{-1}$ ) due to the fluorination,

appearing at 1200 and 1207  $\text{cm}^{-1}$  for *anti* and *syn* isomers, respectively.

While our DFT calculations are performed for an isolated molecule, we find good agreement with the experimental measurements. We also experimentally investigated the possibility of delocalized crystalline vibrational modes. At low Raman shifts, from approximately 300 to 800  $\text{cm}^{-1}$ , we observe weak vibrational modes, with no differences detected for the *syn*, *anti*, or mixed-isomer structures (Supplementary Figure 3). Previous X-ray diffraction (XRD) measurement confirmed that both isomers possess triclinic structures, resulting in P-1 symmetry<sup>25</sup>. Therefore, it is reasonable that there is no differentiation in the Raman spectra for different isomers. Furthermore, the low-frequency Raman responses were much reduced in comparison to the molecular vibration modes. We therefore focus on the higher frequency, localized vibrational modes for our studies of crystalline orientation and isomeric phase coexistence.

**Molecular orientation.** The diF-TES ADT films grown on PFBT-treated Au are highly crystalline, as confirmed by XRD studies<sup>20,24,33</sup>. The narrow linewidths observed in the micro-Raman spectra also indicate high crystallinity, and optical microscope images suggest crystallite sizes on the order of 100  $\mu\text{m}$

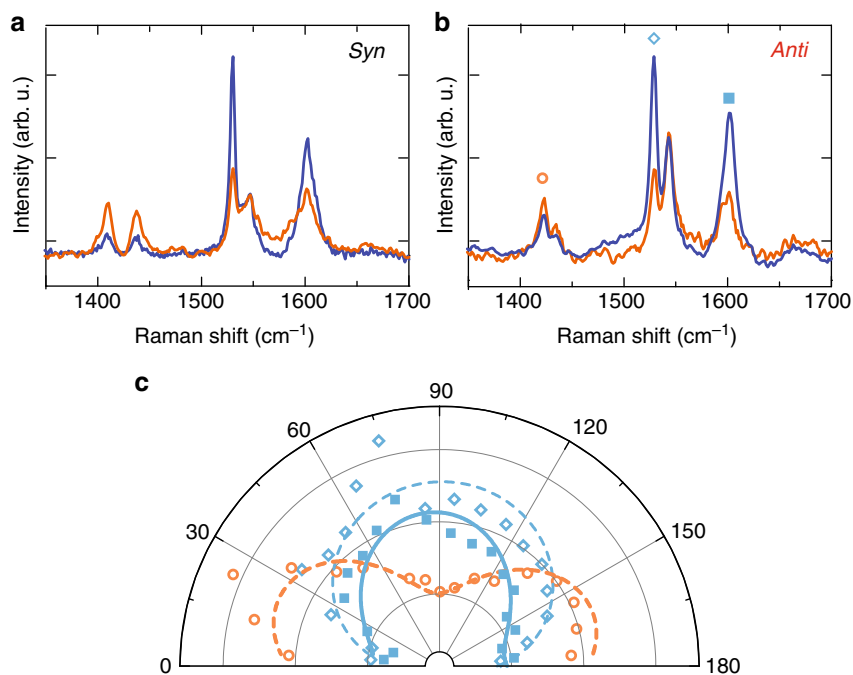


**Fig. 3** Polarized Raman spectra of 2,8-difluoro-5,11-bis(triethylsilylethynyl)anthradithiophene (diF-TES ADT). **a** *Syn* isomer and **b** *anti* isomer with the laser polarization aligned parallel to the C-C long axis ( $\theta = 0^\circ$ , dark blue) and short axis ( $\theta = 90^\circ$ , orange). **c** Polar plot showing the anticorrelation of the short axis ( $1421\text{ cm}^{-1}$ , orange) and long axis ( $1597/1529\text{ cm}^{-1}$ , hollow and solid light blue, respectively) modes for the *anti* isomer in **b**. The lines show fits to  $\cos^2(\theta)$

(Supplementary Figure 4a). The measured micro-Raman spectra do not vary within a crystallite (Supplementary Figure 4b and c). However, while the positions of vibrational modes do not change, the relative intensities of specific modes do vary on adjacent crystallites (Fig. 3a, b). In particular, the long-axis and short-axis vibrational modes are anticorrelated in intensity. Grazing-incidence X-ray diffraction (GIXD) showed that diF-TES ADT adopts an optimal “edge-on” orientation with either one of the silylethynyl side groups adsorbed on the substrate, resulting in the long axis of the conjugated core oriented perpendicular to the plane of the film, as illustrated in Fig. 1b<sup>34</sup>. We therefore attribute the variable intensities of the vibrational modes to changes in the local molecular orientation within the crystallites with respect to the laser polarization. To confirm this hypothesis, we performed angle-dependent polarized Raman spectroscopy, shown for the *anti* isomer in Fig. 3c. When the incident laser polarization aligns parallel to the long axis ( $\theta = 0^\circ$ , blue), a maximum Raman scattering intensity is observed for the  $1597/1529\text{ cm}^{-1}$  modes. The in-phase correlation between the two long-axis vibrational modes was also observed in pentacene characterized by polarization-dependent Raman<sup>35</sup>. The  $1421\text{ cm}^{-1}$  band is in contrast enhanced when the laser polarization is aligned along the short axis ( $\theta = 90^\circ$ , orange). The polarization dependence of the C-C long axis and C-C short axis are therefore  $90^\circ$  out of phase, and both follow the expected  $\cos^2(\theta)$  dependence (Fig. 3c). These results support the anisotropic structure of diF-TES ADT observed in mixed samples using transient absorption microscopy<sup>36</sup>.

**Spatial heterogeneity in mixed sample.** With the ability to spectrally distinguish the *syn* and *anti* isomers, and determine crystallite orientation, we extend our studies to the Raman spectra of mixed diF-TES ADT films. These mixtures of the two isomer structures showed reduced mobility and increased subthreshold slope, resulting in slower turn-on performance in comparison to pure isomer samples<sup>26,27,37</sup>. GIXD revealed a similar structure to

that of single crystals, indicating extended crystalline domains in the thin-film phase, but the spatial extent of these domains has not been determined<sup>18–20,34</sup>. Raman spectra of mixed diF-TES ADT are shown in Fig. 4a. The modes observed appear to be a superposition of the pure isomer spectra, shown in black and red, suggesting there is no intermolecular coupling between the two isomers. The linewidths of the vibrational modes are comparable to those for pure spectra, indicating that long-range order is maintained. This result is in agreement with calculations which found that the two isomers segregate into separate domains where they maintain the local crystalline structure of the pure isomers<sup>27</sup>. We conclude that under the sample preparation conditions for highly ordered films, the mixed sample segregates into pure *syn* and pure *anti* crystallites on length scales shorter than the few hundred nanometer focus region in our experiments.

While the Raman spectra for pure isomers indicated spatially homogeneity within tens to hundreds of micron-sized crystallites, the mixed sample displays significant variations over length scales as short as 200 nm. This can be observed in changes in the relative intensity of the two modes at  $1300\text{ cm}^{-1}$  (Fig. 4b), the three modes close to  $1420\text{ cm}^{-1}$  (Fig. 4c), and the doublet vibrational mode close to  $1540\text{ cm}^{-1}$  (Fig. 4d). Since the long-axis and short-axis vibrational modes ( $1540\text{ cm}^{-1}$ ,  $1420\text{ cm}^{-1}$  respectively) vary significantly in intensity with molecular orientation, as discussed above, we focus on the breathing modes at  $1300\text{ cm}^{-1}$  (*anti*) and  $1286\text{ cm}^{-1}$  (*syn*) as proxies for the pure isomer crystallites.

To resolve the details of the spatial distribution, we performed spectroscopy and imaging of the mixed sample across a  $2 \times 1\ \mu\text{m}^2$  region at 200-nm intervals. Figure 5a shows a contour plot of the spectral region  $1270\text{--}1310\text{ cm}^{-1}$ . Both vibrational modes are consistently resolved in the mixed spectrum, but with variable peak intensity. We are able to resolve correlated changes in the relative intensity of the two vibrational modes. We further extend our analysis to map the integrated intensity ratio  $I_{1300}/I_{1286}$  extracted from these spectra (Fig. 5b). This map demonstrates the

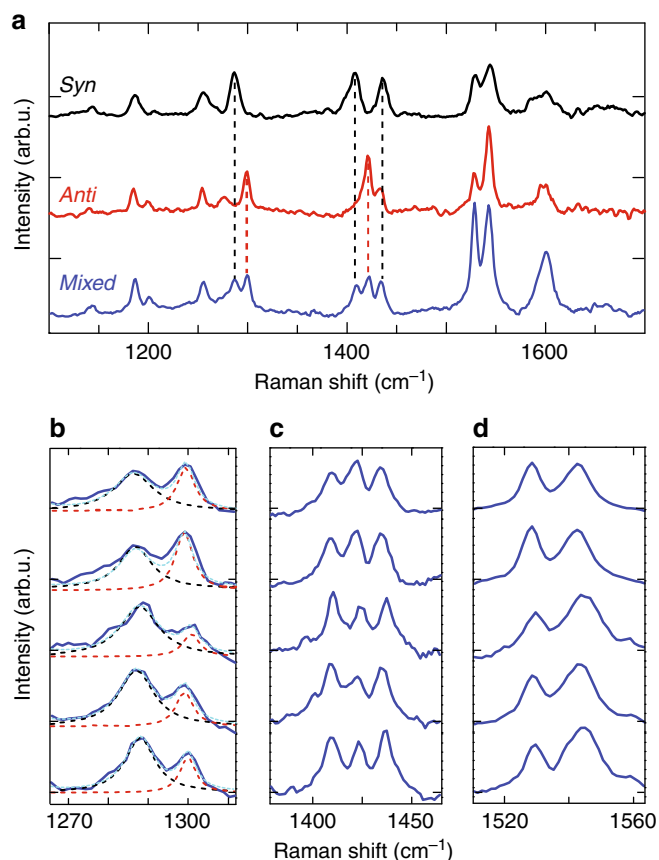


**Fig. 4** Raman spectra of mixed 2,8-difluoro-5,11-bis(triethylsilyl)ethynyl anthradithiophene (diF-TES ADT) thin film. **a** The mixed (blue) spectrum shows the superposition of *syn* (black) and *anti* (red) spectra. **b** Magnification of 1265–1315  $\text{cm}^{-1}$  spectral range, showing changes in relative intensity for ring breathing modes at different locations. The red and black dashed lines show Lorentzian fits to the peaks. **c** Magnification of short-axis vibrational modes in 1375–1475  $\text{cm}^{-1}$  spectral range and **d** long-axis vibrational modes in 1510–1570  $\text{cm}^{-1}$  spectral range

variation of the breathing modes associated with *anti* and *syn* isomers, respectively, with yellow regions indicating a higher proportion of *anti* isomer, and blue regions with more *syn* isomer. Additional intensity maps showing the raw intensities for the 1300 and 1286  $\text{cm}^{-1}$  modes are shown in Supplementary Figure 5a and 5b.

The variation in the spatially distributed spectra and integrated intensity of both vibrational modes indicate that the mixed-isomer films form into homogeneous *anti* and *syn* crystallite sub-domains on length scales below 200 nm. These sub-domains have variable size and local distribution, resulting in superposition spectra with different contributions of *anti* and *syn* spectral signatures, as resolved in Figs. 4 and 5. As we observe no regions with only one of the 1286 or 1300  $\text{cm}^{-1}$  vibrational modes, we conclude that the pure isomer sub-domains have spatial extent significantly below the 200-nm step size measured here, possibly on the order of tens of nanometers. Higher spatial resolution techniques are therefore necessary to directly resolve the pure isomer domains.

It is important to note that our observations of isomeric segregation based on Raman spectroscopy apply to the highly ordered structures arising from SAC deposition. This deposition method is known to produce high crystallinity and therefore favorable mobilities, in particular in pure isomer systems. Other

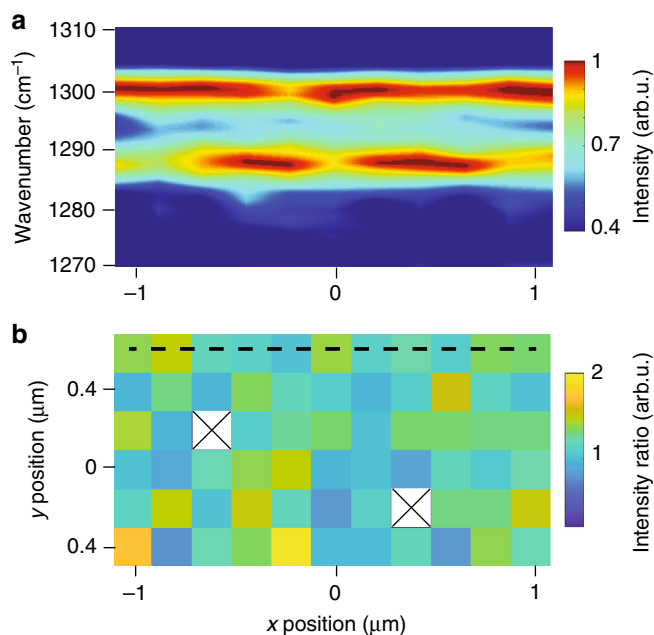


**Fig. 5** Spatial distribution of mixed-isomer sample. **a** Contour plot showing correlated changes in peak intensity at 1300 and 1286  $\text{cm}^{-1}$  for spectra taken at 200-nm intervals. **b** Integrated intensity ratio for peaks at 1300 and 1286  $\text{cm}^{-1}$ . The ratio  $I_{1300}/I_{1286}$  represents the relative quantity of *anti* to *syn* molecules in the laser probe volume. The dashed line indicates the spectra shown in **a**. The two white boxes indicate points where poor signal led to excessive noise in the integrated intensity

thin-film preparations, for example, rapid spin casting, would lead to lower molecular order and therefore reduced phase separation<sup>29</sup>. Raman spectroscopy can provide valuable information about the degree of order in organic semiconductors, but is additionally helpful in characterizing isomer distribution in highly crystalline systems to optimize mobilities for high-performance applications.

## Discussion

Micro-Raman spectroscopy is a powerful technique to investigate crystalline order in molecular systems. Here, we demonstrate its use for characterizing the spatial properties of a mixed-isomer organic small-molecule semiconductor, diF-TES ADT, through the spectroscopic signatures of the pure isomers. Our results indicate that crystallites of isomeric purity coexist intimately, while maintaining their high crystallinity and orientational order, even across sub-domains. This phase segregated behavior explains the reduction in mobility and slower turn-on response observed in mixed diF-TES ADT TFTs, with grain boundaries between crystallites potentially introducing defects and reducing the efficiency of charge transfer in spite of their high crystallinity. The ability to spectrally discriminate isomer crystallites and their heterogeneous distribution and packing is important to optimize thin-film preparation in this small-molecule semiconductor, and can also provide information about isomer microstructure in other small molecules. These results highlight the importance of thin-film preparation for control of isomer distribution and domain engineering, and provide a means to characterize and optimize device performance.

## Methods

**Sample preparation.** The pure form *syn* and *anti* diF-TES ADT and 50–50 mixtures of isomers were synthesized by a previously reported method<sup>26</sup>.  $n++$ -doped Si with 200 nm of thermally oxidized  $\text{SiO}_2$  was used as the underlying substrate. Contacts patterned by photolithography were deposited by electron



beam evaporation of 5 nm of Ti followed by 45 nm of Au. The substrates were cleaned by soaking in hot acetone, then hot isopropyl alcohol for 10 min each, followed by a 10-min exposure to ultraviolet/ozone and a rinse with deionized water. Upon drying, the substrates were soaked in 30 mM solutions of PFBT in room-temperature ethanol for 30 min, followed by a 5-min sonication in fresh ethanol to remove any excess PFBT. Substrates with Au features were necessary in order to obtain a highly ordered film with molecular orientation out of plane (Fig. 1b), as we have explained in detail elsewhere<sup>33</sup>. Solutions of 0.3% w/w diF-TES ADT in chlorobenzene were drop cast on these substrates and placed in a closed Petri dish with an additional 250  $\mu$ L of chlorobenzene, creating a solvent-rich environment. The thin films were formed after the solvents were allowed to evaporate over 1–2 days.

**Raman spectroscopy.** Micro-Raman spectra were acquired using a Renishaw inVia Raman microscope with 488-nm laser excitation (objective 0.75 NA Olympus,  $\times 50$ ). The corresponding lateral resolution of the beam spot was around 0.32  $\mu$ m<sup>2</sup>, defined by  $\lambda/(2NA)$ . All samples were measured in air. Spectra were averaged for 20 accumulations each with 2-s duration. In polarized Raman spectra, a half-wave plate was placed between the laser and the sample to control the incident polarization (Fig. 1b). Two-dimensional mapping of the mixed sample was performed using a Horiba LabRAM HR Evolution Raman microscope with 473-nm laser excitation (objective 0.9 NA Olympus,  $\times 100$ ). The corresponding lateral resolution was around 0.26  $\mu$ m<sup>2</sup>. The spectra were collected 200 nm apart, with each point averaged for two accumulations with 5-s duration.

**DFT calculation.** DFT calculations were performed with the GAUSSIAN09 software. The geometry of a symmetric segment was first optimized, then frequency analysis was performed using the B3LYP hybrid functional, and the 6-31G(d) basis set. The frequencies were scaled by a factor of 0.96 for comparison. The molecular core is defined as the conjugated fused acene rings. The *anti* isomer has a core with  $C_{2h}$  symmetry, with the two sulfurs in thiophene rings in inversion correlation. The core of the *syn* isomer has  $C_{2v}$  symmetry.

## Data availability

The authors declare that the data within the article and Supplementary Information, as well as additional data supporting the findings of this study, are available upon reasonable request.

Received: 7 June 2018 Accepted: 30 January 2019

Published online: 25 February 2019

## References

1. Sekitani, T., Zschieschang, U., Klauk, H. & Someya, T. Flexible organic transistors and circuits with extreme bending stability. *Nat. Mater.* **9**, 1015–1022 (2010).
2. Gelinck, G., Heremans, P., Nomoto, K. & Anthopoulos, T. D. Organic transistors in optical displays and microelectronic applications. *Adv. Mater.* **22**, 3778–3798 (2010).
3. Ward, J. W., Lampion, Z. A. & Jurchescu, O. D. Versatile organic transistors by solution processing. *ChemPhysChem* **16**, 1118–1132 (2015).
4. Heremans, P. et al. Mechanical and electronic properties of thin-film transistors on plastic, and their integration in flexible electronic applications. *Adv. Mater.* **28**, 4266–4282 (2016).
5. Chabinyc, M. L., Toney, M. F., Kline, R. J., McCulloch, I. & Heeney, M. X-ray scattering study of thin films of poly(2,5-bis(3-alkylthiophen-2-yl)thieno[3,2-b]thiophene). *J. Am. Chem. Soc.* **129**, 3226–3237 (2007).
6. Mas-Torrent, M. & Rovira, C. Role of molecular order and solid-state structure in organic field-effect transistors. *Chem. Rev.* **111**, 4833–4856 (2011).
7. Rivnay, J., Mannsfeld, S. C. B., Miller, C. E., Salleo, A. & Toney, M. F. Quantitative determination of organic semiconductor microstructure from the molecular to device scale. *Chem. Rev.* **112**, 488–5519 (2012).
8. Hiszpanski, A. M. et al. Tuning polymorphism and orientation in organic semiconductor thin films via post-deposition processing. *J. Am. Chem. Soc.* **136**, 15749–15756 (2014).
9. Giri, G. et al. One-dimensional self-confinement promotes polymorph selection in large-area organic semiconductor thin films. *Nat. Commun.* **5**, 3573 (2014).
10. Goetz, K. P. et al. Freezing-in orientational disorder induces crossover from thermally-activated to temperature-independent transport in organic semiconductors. *Nat. Commun.* **5**, 5642 (2014).
11. Schweicher, G. et al. Bulky end-capped [1]benzothieno[3,2-b]benzothiophenes: reaching high-mobility organic semiconductors by fine tuning of the crystalline solid-state order. *Adv. Mater.* **27**, 3066–3072 (2015).
12. Richter, L. J., Delongchamp, D. M. & Amassian, A. Morphology development in solution-processed functional organic blend films: an in situ viewpoint. *Chem. Rev.* **117**, 6332–6366 (2017).
13. Anthony, J. E. Functionalized acenes and heteroacenes for organic electronics. *Chem. Rev.* **106**, 5028–5048 (2006).
14. Mamada, M. et al. Syn-/anti-anthradithiophene derivative isomer effects on semiconducting properties. *ACS Appl. Mater. Interfaces* **5**, 9670–9677 (2013).
15. Dickey, K. C., Anthony, J. E. & Loo, Y. L. Improving organic thin-film transistor performance through solvent-vapor annealing of solution-processable triethylsilylthiophenyl anthradithiophene. *Adv. Mater.* **18**, 1721–1726 (2006).
16. Chen, J. et al. Solvent-type-dependent polymorphism and charge transport in a long fused-ring organic semiconductor. *Nanoscale* **6**, 449–456 (2014).
17. Subramanian, S. et al. Chromophore fluorination enhances crystallization and stability of soluble anthradithiophene semiconductors. *J. Am. Chem. Soc.* **130**, 2706–2707 (2008).
18. Jurchescu, O. D. et al. Organic single-crystal field-effect transistors of a soluble anthradithiophene. *Chem. Mater.* **20**, 6733–6737 (2008).
19. Gundlach, D. J. et al. Contact-induced crystallinity for high-performance soluble acene-based transistors and circuits. *Nat. Mater.* **7**, 216–221 (2008).
20. Ward, J. W. et al. Tailored interfaces for self-patterning organic thin-film transistors. *J. Mater. Chem.* **22**, 19047–19053 (2012).
21. Diemer, P. J. et al. Quantitative analysis of the density of trap states at the semiconductor-dielectric interface in organic field-effect transistors. *Appl. Phys. Lett.* **107**, 103303 (2015).
22. Mei, Y. et al. Interface engineering to enhance charge injection and transport in solution-deposited organic transistors. *Org. Electron.* **50**, 100–105 (2017).
23. Mei, Y. et al. Crossover from band-like to thermally activated charge transport in organic transistors due to strain-induced traps. *Proc. Natl. Acad. Sci. USA* **114**, E6739–E6748 (2017).
24. Ward, J. W. et al. Rational design of organic semiconductors for texture control and self-patterning on halogenated surfaces. *Adv. Funct. Mater.* **24**, 5052–5058 (2014).
25. Lehnher, D. et al. Isomerically pure *syn*-anthradithiophenes: synthesis, properties, and FET performance. *Org. Lett.* **14**, 3660–3663 (2012).
26. Hallani, R. K. et al. Structural and electronic properties of crystalline, isomerically pure anthradithiophene derivatives. *Adv. Funct. Mater.* **26**, 2341–2348 (2016).
27. Diemer, P. J. et al. The influence of isomer purity on trap states and performance of organic thin-film transistors. *Adv. Electron. Mater.* **3**, 1600294 (2017).
28. Park, S. K., Mourey, D. A., Subramanian, S., Anthony, J. E. & Jackson, T. N. High-mobility spin-cast organic thin film transistors. *Appl. Phys. Lett.* **93**, 2006–2009 (2008).
29. Diemer, P. J. et al. Vibration-assisted crystallization improves organic/dielectric interface in organic thin-film transistors. *Adv. Mater.* **25**, 6956–6962 (2013).
30. Furukawa, Y. et al. Infrared and Raman spectroscopy of organic thin films used for electronic devices. *Vib. Spectrosc.* **60**, 5–9 (2012).
31. Chen, C. Y. et al. Understanding the interplay between molecule orientation and graphene using polarized Raman spectroscopy. *ACS Photonics* **3**, 985–991 (2016).
32. Yamakita, Y., Kimura, J. & Ohno, K. Molecular vibrations of [*n*]oligoacenes (*n* = 2–5 and 10) and phonon dispersion relations of polyacene. *J. Chem. Phys.* **126**, 064904 (2007).
33. Li, R. et al. Direct structural mapping of organic field-effect transistors reveals bottlenecks to carrier transport. *Adv. Mater.* **24**, 5553–5558 (2012).
34. Kline, R. J. et al. Controlling the microstructure of solution-processable small molecules in thin-film transistors through substrate chemistry. *Chem. Mater.* **23**, 1194–1203 (2011).
35. Kang, C. M. et al. 1 GHz pentacene diode rectifiers enabled by controlled film deposition on SAM-treated Au anodes. *Adv. Electron. Mater.* **2**, 1500282 (2016).
36. Wong, C. Y., Folie, B. D., Cotts, B. L. & Ginsberg, N. S. Discerning variable extents of interdomain orientational and structural heterogeneity in solution-cast polycrystalline organic semiconducting thin films. *J. Phys. Chem. Lett.* **6**, 3155–3162 (2015).
37. Hailey, A. K. et al. Understanding the crystal packing and organic thin-film transistor performance in isomeric guest–host systems. *Adv. Mater.* **29**, 1700048 (2017).
38. James, D. T. et al. Thin-film morphology of inkjet-printed single-droplet organic transistors using polarized Raman spectroscopy: effect of blending TIPS-pentacene with insulating polymer. *ACS Nano* **5**, 9824–9835 (2011).
39. Wood, S. et al. Precise characterisation of molecular orientation in a single crystal field-effect transistor using polarised Raman spectroscopy. *Sci. Rep.* **6**, 33057 (2016).

## Acknowledgements

A portion of this work was performed using the Raman microspectrometer in the UNC EFRC Instrumentation Facility established by the UNC EFRC Center for Solar Fuels, an Energy Frontier Research Center funded by the US Department of Energy, Office of Science, Office of Basic Energy Sciences under Award DE-SC0001011. P.J.D. and O.D.J. acknowledge support from the NSF ECCS 1254757. A.J.P. and J.E.A. thank NSF DMREF-162748 for support. We also thank Prof. Kizhanipuram Vinodgopal for allowing us to use the Raman microspectrometer at North Carolina Central University.

## Author contributions

The experiments were conceived by J.M.A. and O.D.J. C.-W.H. performed the experiments, implemented the calculations, and analyzed the data, with help from X.Y. P.J.D. prepared the crystalline films. A.J.P. and J.E.A. synthesized the pure isomers and the mixed molecules. C.-W.H. and J.M.A. wrote the manuscript, with input from all authors. J.M.A. supervised the project.

## Additional information

**Supplementary information** accompanies this paper at <https://doi.org/10.1038/s42004-019-0122-7>.

**Competing interests:** The authors declare no competing interests.

**Reprints and permission** information is available online at <http://npg.nature.com/reprintsandpermissions/>

**Publisher's note:** Springer Nature remains neutral with regard to jurisdictional claims in published maps and institutional affiliations.



**Open Access** This article is licensed under a Creative Commons Attribution 4.0 International License, which permits use, sharing, adaptation, distribution and reproduction in any medium or format, as long as you give appropriate credit to the original author(s) and the source, provide a link to the Creative Commons license, and indicate if changes were made. The images or other third party material in this article are included in the article's Creative Commons license, unless indicated otherwise in a credit line to the material. If material is not included in the article's Creative Commons license and your intended use is not permitted by statutory regulation or exceeds the permitted use, you will need to obtain permission directly from the copyright holder. To view a copy of this license, visit <http://creativecommons.org/licenses/by/4.0/>.

© The Author(s) 2019